ACS APPLIED MATERIALS & INTERFACES

Research Article

Cite This: ACS Appl. Mater. Interfaces 2020, 12, 1895−1904

www.acsami.org

Ultralow-Voltage-Driven Smart Control of Diverse Drop's Anisotropic Sliding by in Situ Switching Joule Heat on Paraffin-Infused Microgrooved Slippery Surface

Chao Chen,[†] Lili Zhou,[‡] Lu-An Shi,[§] Suwan Zhu,[†] Zhouchen Huang,[†] Cheng Xue,[†] Jiawen Li,[†] Yanlei Hu,*[,†] Dong Wu,*[,†] and Jiaru Chu[†]

[†]CAS Key Laboratory of Mechanical Behavior and Design of Materials, Department of Precision Machinery and Precision Instrumentation, University of Science and Technology of China, Hefei 230026, China

[‡]School of Instrument Science and Optoelectronics Engineering, Hefei University of Technology, Hefei 230009, China

[§]Division of Nanomaterials and Chemistry, Hefei National Laboratory for Physical Sciences at the Microscale, Collaborative Innovation Center of Suzhou Nano Science and Technology, CAS Center for Excellence in Nanoscience, Hefei Science Center of CAS, Department of Chemistry, University of Science and Technology of China, Hefei 230026, China

Supporting Information

ABSTRACT: Stimuli-responsive anisotropic slippery surfaces (ASSs) have demonstrated intriguing performance in manipulating the behaviors of some liquids. However, most present methods have been limited to conductive droplets, certain specific conductive platforms, and higher manipulation temperature that greatly hinder its practical applications. Here, an electric-responsive paraffin-infused ASS (ER-PIASS) composed of paraffin, microgrooved PDMS, and flexible embedded silver nanowire heater is reported. Owing to the fast electric-response of ER-PIASS, smart control between anisotropic sliding and pinning for diverse liquids can be realized by remotely loading and discharging electric-stimuli. The underlying mechanism is that the generated Joule heat melts the solidified paraffin to slide a pinning droplet once an electric-trigger is loaded due to the formation of a slippery air/liquid/liquid/solid system. Once the voltage is discharged, the liquefied paraffin would rapidly solidify to stick to a slipping droplet because of the recovery of a frictional air/liquid/solid system. Additionally, the effect of the groove's height (h), spacing between two adjacent grooves (d), and thickness of the paraffin layer on the anisotropic degree was quantitatively studied and an optimized value of 75° is thus harvested. Through tuning the recipe of the hybrid lubricant, the responsive voltage and temperature for ER-PIASS can be dramatically decreased to ultralow figures of 2.0 V and 34.2 °C. By taking advantage of this ultralow-voltage-driven biocompatible ER-PIASS, we enable the anisotropic smart control of cell culture medium and yeast droplets for their directional coalesce, growth, and fission. We believe that such stimuli-responsive surfaces will be promising candidates for manipulating droplets' directional sliding behavior and further bloom the studies of flexible microfluidics devices.

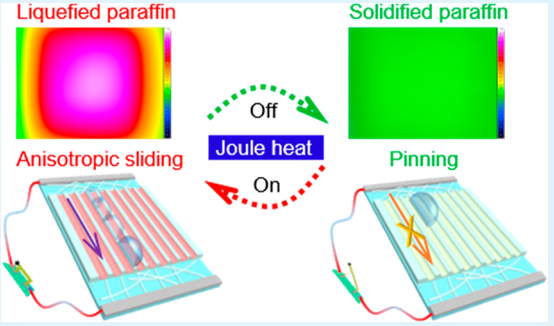

KEYWORDS: *ultralow-voltage-responsive anisotropic slippery surface, femtosecond laser programmable scanning, silver nanowire heater, switchable wettability, cell culture*

1. INTRODUCTION

In the past decades, slippery lubricant-infused porous surfaces (SLIPS) inspired by *Nepenthes* pitcher plants, which has apparent advantages of excellent defect tolerance,[1] low contact angle (CA) hysteresis[2] and super-repellency against immiscible liquids,[3] have aroused tremendous attentions in the fields of chemistry and materials because of their potential applications in droplet and bubble manipulation,[4,5] oil−water separation,[6,7] enhancement of dropwise condensation,[8,9] drag reduction,[10] antifouling,[11−13] anti-icing,[14−16] anticorrosion,[17] and biomedical engineering.[18] Typically, via the incorporation of rice leaflike aligned anisotropic surfaces and SLIPS, people have realized the intentional transport of diverse liquids by taking advantages of many artificial anisotropic slippery surfaces (ASSs),[19,20] which have profound significance for water-directional collection, drag reduction and microfluidic devices. Unfortunately, these stiff ASSs can only guide the microdroplets along the as-designed routes incessantly,[21−25] it is therefore a challenge to prepare smart ASSs for achieving the dynamic control of a drop's anisotropic sliding motion.

To overcome this limitation, Jiang and his co-workers have paved great efforts to develop responsive ASSs with multi-

Received: October 4, 2019
Accepted: December 3, 2019
Published: December 3, 2019

DOI: 10.1021/acsami.9b17936
ACS Appl. Mater. Interfaces 2020, 12, 1895−1904

Table 1. Comparisons of Key Parameters for Stimuli-Responsive ASSs

materials	method	conditions	response	control manner	$SA_{\perp} - SA_{//}$	ref.
directional P3HT film/silicone oil	freeze-drying	liquid nitrogen/vacuum	electric	contact	<30°	26
directional rGO film/silicone oil	freeze-drying	liquid nitrogen/vacuum	electric	contact	<25°	27
directional PCDTPT film/silicone oil	freeze-drying	liquid nitrogen/vacuum	electric	contact	<30°	28
directional PS film/paraffin	freeze-drying	liquid nitrogen/vacuum	thermal (ex-situ hot plate)	contactless	<30°	29
directional P3HT/PCBM film/silicone oil	one-step femtosecond laser ablation	liquid nitrogen/vacuum	photoelectric synergetic	contact	<30°	30
microgrooved PDMS/paraffin/underlying SNWH	one-step femtosecond laser ablation	ambient	electro-thermal (in situ Joule heat)	remotely contactless	72°	this work

functionalities. For example, Guo et al. prepared an electrically responsive slippery surfaces by virtue of infusing silicone oil into a conductive anisotropic porous poly(3-hexylthiophene) (P3HT) film, and then the motion of conductive liquid droplets could be reversibly controlled between sliding and pinning on this smart ASS by alternating on−off voltages.[26] On this basis, by infusing the conductive lubricant oil into the porous, conductive and anisotropic reduced graphene oxide (rGO) film, Che et al. could further reduce the responsive voltage of electrically driven droplet motion.[27] Then, Wang et al. deployed a further study to clarify the influence of lubricant viscosity and thickness on the electro-responsive behavior and self-healing performance of ASS, where they demonstrated that the critical self-healing thickness tended to elevate with increasing silicone oil viscosity and the lower-viscosity silicone oils lubricating in the porous ASS could reduce the responsive voltage of the electrical control of droplet motion.[28] Furthermore, Wang et al. fabricated a temperature-responsive ASS through the combination of directional porous polystyrene (PS) films by a one-step freeze-drying method and lubricated paraffin, which was utilized for the temperature-driven smart control of the anisotropic motion of the droplets.[29] More recently, they reported a photoelectric synergetic responsive ASS by using a poly(3-hexylthiophene-2,5-diyl)/[6,6]-phenyl-C_{61}-butyric acid methyl ester (P3HT/PCBM) binary system, which could serve for the photoelectric synergetic control of droplet anisotropic sliding and interfacial sentinel oxidative degradation.[30] In brief, the previous investigations have greatly inspired the theoretical understanding and experimental guidance for achieving the dynamic control of a drop's motion on smart responsive ASSs. However, several severe drawbacks, unfortunately, are still delusory. (1) ASSs were always harvested from a freeze-drying method, where the extremely harsh environment (e.g., liquid nitrogen, vacuum ambiance) and the tedious frozen process (e.g., overnight) are apparently demanding and inefficient.[26−30] (2) To realize anisotropic smart control of a drop's sliding, two typical criteria of conductive liquids and conductive anisotropic porous substrate must be satisfied, signifying that this system is only limited to special liquids and materials but not widely adaptive for other ones.[26−28,30] (3) The sliding angle (SA) difference between the parallel direction ($SA_{//}$) and the perpendicular direction ($SA_{\perp}$) are too small to guarantee its anisotropic degree (Table 1).[26−30] (4) Previous study over paraffin infused ASS is always subject to ex situ and rigid heating sources (e.g., air oven, 220 V).[29] (5) In situ contactless control of a drop's sliding (e.g., pinning and sliding) has not been realized on flexible 3D surface.[26−30] (6) Though the dynamic control for diverse liquids on isotropic SLIPS has been realized in our previous study, the higher manipulation temperature (64 °C) can easily lead to the severe volatilization and degradation for droplets, especially for lower surface tension species.[39] To the best of our knowledge, room temperature-responsive anisotropic surfaces have rare investigations. In this regard, it is still a timely challenge and urgent need to explore a more facile method for the fabrication of a low-temperature-responsive ASS with excellent anisotropic degree, which is widely adaptive for remotely controlling diverse drop's sliding behavior on 2D/3D surfaces.

Here, we first report an electric-responsive paraffin-infused anisotropic slippery surface (ER-PIASS) by incorporation of phase-change-material (PCM) of paraffin wax, periodic micro-grooved (MG) PDMS that are fabricated using one-step programmable femtosecond laser scanning, and an embedded flexible silver nanowire heater (SNWH). By remotely loading/discharging an electric-trigger, the dynamic control between anisotropic sliding and pinning for diverse liquids is realized. The underlying mechanism is that the generated Joule heat tends to melt the surface paraffin of ER-PIASS within 20 s for a slippery air/liquid/liquid/solid (ALLS) system when we remotely apply an electric-stimuli (5 V). Once the voltage is intentionally switched off, the melt paraffin would rapidly solidify to a frictional air/liquid/solid (ALS) system within 10 s through the heat transfer process so as to brake a moving droplet on ER-PIASS. This electric-induced heating device can be widely adaptive for a variety of materials, which is crucial for broad applications. Additionally, we quantitatively study the effect of laser power, MG distance, thickness of the top paraffin layer, and drop volume on the anisotropic degree of the resultant ER-PIASSs. Through tuning the doping content of liquid paraffin in the hybrid lubricant, the ER-PIASS dramatically unfolds a room-temperature-responsive property at an ultralow voltage of 2 V. Moreover, owing to its excellent flexibility, in situ anisotropic manipulation of functionalized droplets on a curved ER-PIASS for metachromatism is successfully deployed. Significantly, due to its low-temperature-driven merit and good biocompatibility, smart ER-PIASS is competent for intentional transport of nonconductive biological ones or conductive ionic droplets. This work provides insights for dealing with the challenges of stimuli-responsive anisotropic surfaces.

2. RESULTS AND DISCUSSION

2.1. Facile Fabrication of Smart ER-PIASS and Its Characterizations. To achieve the anisotropic sliding of a droplet, the hydrophobic anisotropic platform was always considered as a prerequisite,[2] which could prevent the targeted liquids from the intrusion into the interface between the lubricant oil and the solid platform and endow the difference of $SA_{//}$ and $SA_{\perp}$ ($SA_{//} - SA_{\perp}$) with remarkable discrepancy. In this

DOI: 10.1021/acsami.9b17936
ACS Appl. Mater. Interfaces 2020, 12, 1895−1904

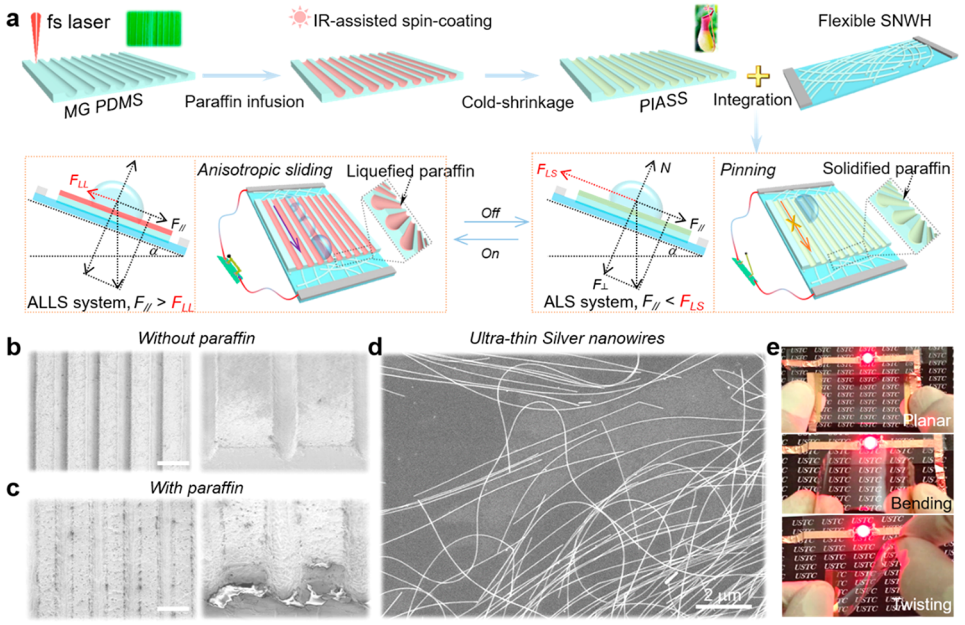

Figure 1. Facile fabrication of Joule-heat-switching ER-PIASS and its characterizations. (a) Schematic diagram for illustrating the fabricating strategy of ER-PIASS composed of one-step femtosecond laser scanning of MG PDMS, thermal-spin-coating of paraffin wax, and integration of an embedded SNWH, in addition to the mechanism of realizing the smart control of a drop's anisotropic sliding. SEM images for MG PDMS (b) without and (c) with the paraffin lubrication; scale bar is 100 μm. (d) SEM image for characterizing the length of the as-prepared silver nanowires by a polyol method. (e) Clips for displaying the flexible performance of the resultant SNWH.

regard, one-step femtosecond laser scanning, which could easily modify the wettability for diverse materials such as polymers and metals through introducing the micro- and nanostructures,[31−34] was therefore adopted for fabricating a kind of rice leaflike MG array decorated with plenty of nanoparticles and nanopores on the as-prepared PDMS (Figure 1a and Figure S1). The typical width (w), depth (h), and distance between two adjacent MGs (d) were measured as 70, 50, and 100 μm (Figure 1b and Figure S2), respectively. Thereafter, the thermal-spin-coating method was first explored for the anisotropic uniform spreading of the melt paraffin on the MG PDMS, where the melt temperature (T_m) for this commercial paraffin was received as 42−45 °C (Figure 1c and Figure S3). After a cold-shrinkage treatment, temperature-responsive paraffin-infused anisotropic slippery surface (PIASS) could be successfully harvested. Actually, paraffin with other T_m values can be used according to specific requirements in practical applications by virtue of adjusting the ratio between the solid paraffin and doped liquid paraffin.[35,36] Moreover, current surfaces also exhibited an anisotropic wettability, where the water contact angle in the parallel ($WCA_{//}$) and perpendicular ($WCA_{\perp}$) directions for PIASS were measured as 105° and 120° in comparison with that for pristine MG PDMS as 123° and 135° (Figure S4). Then, ultrathin silver nanowires with the diameter of ∼20 nm (Figure S5) and length of ∼20 μm could be synthesized by a classical polyol method,[37−39] which could be uniformly coated on PET substrate for a transparent conductive film (TCF) (Figure 1d and Figure S6). Electric-triggered silver nanowire heater (SNWH) could be easily obtained through the introduction of two symmetric copper wires by two pieces of organized oblong silver paste, which unfolded excellent flexibility, high-transparency, and mechanical stability (Figure 1e; Movie S1, Supporting Information). Finally, smart ER-PIASS could be facilely integrated by temperature-responsive PIASS and an underlying embedded SNWH through a thin layer of PDMS binder.

Upon this quaternary droplet actuator composed of aligned paraffin wax, anisotropic MG PDMS, PDMS binder, and electric-triggered SNWH, we could dramatically achieve the in situ dynamic control of a drop's anisotropic sliding behavior by alternately applying and discharging Joule heat. The surface temperature of smart ER-PIASS (T) was lower than T_m when the voltage is switched off, that is, at $T < T_m$, the solidified paraffin was responsible for a frictional air/liquid/solid (ALS) system in the parallel direction. So, the droplet in contact with this surface, which was supported by rough and wrinkled paraffin, tended to pin in the Wenzel state. Here, the frictional resistance (F_{LS}) is defined as the frictional force between the liquid droplet (L) and the solidified wrinkled paraffin wax (S). In contrary, once we intentionally triggered Joule heat by in situ loading an electric-stimuli, the melt paraffin should contribute to a slippery air/liquid/liquid/solid (ALLS) system in the parallel direction for sliding a pinning droplet. In short, we can remotely steer a drop's dynamic control between anisotropic sliding and pinning by selectively applying/discharging an electric-trigger, that is, generating/removing Joule heat for the conversion between frictional ALS and slippery ALLS system. In terms of microgroove's effect, it enables both the anisotropic distribution of paraffin wax and the anisotropic energy barrier (Figure S7). The lower microgrooved channel (paraffin-rich valley) is capable of capturing and storing more lubricant than the upper exposed segment (paraffin-lacking plateau), which contributes to the anisotropic sliding state in response to electric-stimuli. In addition, the fluctuant terrain along the y-axis leads to much larger energy barrier, a higher contact angle hysteresis (CAH), and a very hard slide in comparison with those of the even topography along x-axis. More significantly, the anisotropic sliding of droplet is dominated by the anisotropic grooves. Loading/discharging Joule heat is only capable of

DOI: 10.1021/acsami.9b17936
ACS Appl. Mater. Interfaces 2020, 12, 1895−1904

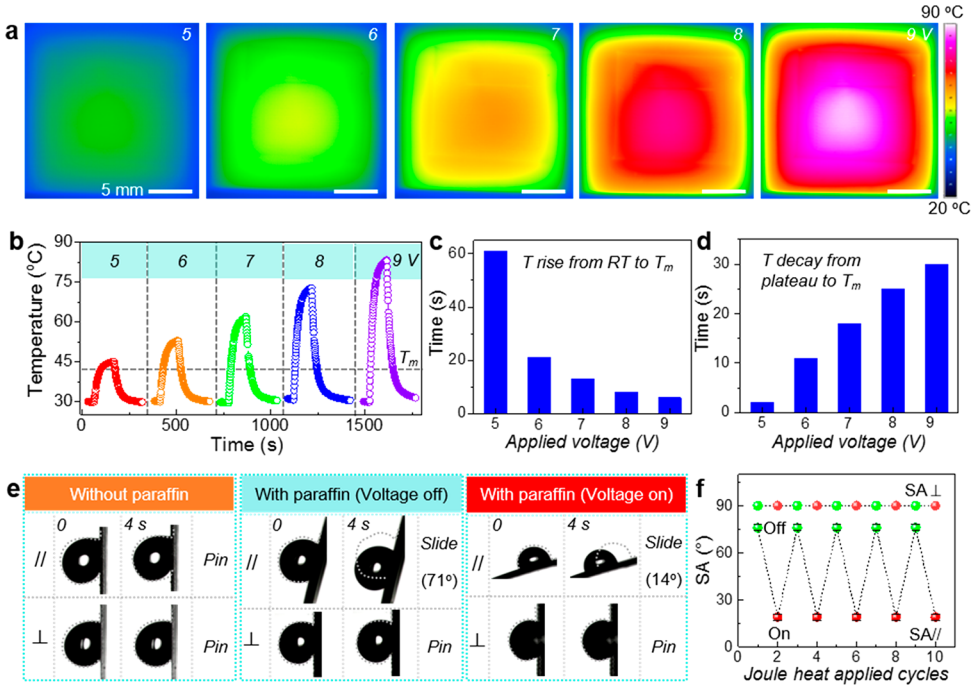

Figure 2. In situ switchable adhesion by switching electric-trigger. (a) IR images for representing the temperature distribution on Joule-heated ER-PIASS in response to the voltages of 4, 5, 6, 7, and 8 V, respectively. (b) Temperature−time curves for ER-PIASS under different electric-triggers. Time variations of the temperature of smart ER-PIASS (c) rising from RT to T_m and (d) decaying from $T_{plateau}$ to T_m with the change of serving voltages. (e) Comparison of a water drop's (5 μL) adhesion on pristine MG PDMS, untriggered ER-PIASS, and Joule-heated PIASS. (f) Reversible adhesions for water droplets on smart ER-PIASS by in situ manipulating the on−off switch of a pulsed electric-stimuli (5 V).

realizing the motion control between pinning and sliding along x-axis direction. For y-axis dimension, however, the droplet tends to invariably stick whether the surface paraffin is melted or solidified because of giant groove's energy barrier and viscous force. In summary, the mechanism of anisotropic sliding motion control is determined by the anisotropic grooves, anisotropic energy barrier and the anisotropic distribution of lubricant paraffin wax in addition to the transition of paraffin state along x-axis direction between the liquid and solid in response to Joule heat.

2.2. In Situ Switchable Adhesion of ER-PIASS by Remotely Modulating Joule-Heat. As an intelligent electric-triggered actuator, the as-prepared ER-PIASS should account for the uninterrupted anisotropic transportation of a targeted droplet, which highly demands the homogeneous generation of Joule heat for an even slippery surface. According to the feedback of an infrared radiation (IR) imager in Figure 2a, we convinced that the periodic solid paraffin wax was capable of melting uniformly due to the homogeneous formation of Joule heat. The larger the served voltage, the more the generated Joule heat and the higher the induced local temperature (Figure 2b). Considering that the generated Joule heat marched successively from the underlying SNWH toward anisotropic MG PDMS and the then top paraffin layer, the rising (voltage on) and decaying (voltage off) time of the surface temperature for ER-PIASS were determined by a time constant of transient thermal response (τ) that is equal to $\rho dc/h$.[40] Therein, ρ, d, c, and h represent the mass density, thickness, specific heat capacity, and heat-transfer coefficient, respectively. Accordingly, the generated Joule heat transferred from the underlying SNWH to the top paraffin layer using 61, 21, 13, 8, and 6 s for elevating the temperature above T_m when we loaded a series of voltages at 4, 5, 6, 7, and 8 V (Figure 2c). The larger the applied voltage, the shorter the thermal rising time. In sharp contrast, the corresponding decaying time increased from 2 to 11, 18, 25 and then 30 s for decreasing the surface temperature of ER-PIASS below T_m (Figure 2d). The larger the served voltage, the higher the temperature plateau and the slower the thermal decaying time. On this basis, people could select a desirable serving voltage according to one's practical requirement. In the current work, we adopted the serving voltage of 5 V with respect to its moderate thermal response time.

By virtue of remotely switching Joule heat, the drop's adhesion on smart ER-PIASS could be flexibly regulated via tuning the frictional resistance in the parallel direction ($f_{//}$). As shown in Figure 2e, water droplets (5 μL) tended to pin on a raw MG PDMS without the lubrication of paraffin even though it had been tilted to 90°, because their gravity force is not capable of overcoming either $f_{//}$ or $f_{\perp}$. In comparison, the sliding angle in the parallel orientation ($SA_{//}$) for droplets on smart ER-PIASS could be in situ switchable between 76° and 19° by simply discharging and loading voltage whereas it was inclined to stick invariably in the perpendicular direction. As a result, the anisotropic degree ($SA_{\perp}$- $SA_{//}$) could be reversibly switched between 14° and 71° by taking advantage of discharging and triggering electric-stimuli (Figure 2f).

2.3. Anisotropic Performance Optimization for Droplets on Joule-Heated ER-PIASS. Considering that the anisotropic performance ($\Delta SA = SA_{\perp} - SA_{//}$) for droplets on Joule-heated ER-PIASS should be highly dependent on the topography of MG PDMS, which actually dominated the thickness of the top paraffin layer. Here, we quantitatively studied the effect of laser scanning power (P), thermal-spin-coating speed (v) and dosage (τ), distance between two adjacent MGs (d), and drop volume (V) on the ΔSA values for droplets on Joule-heated ER-PIASS. With the increase of P, the

DOI: 10.1021/acsami.9b17936
ACS Appl. Mater. Interfaces 2020, 12, 1895−1904

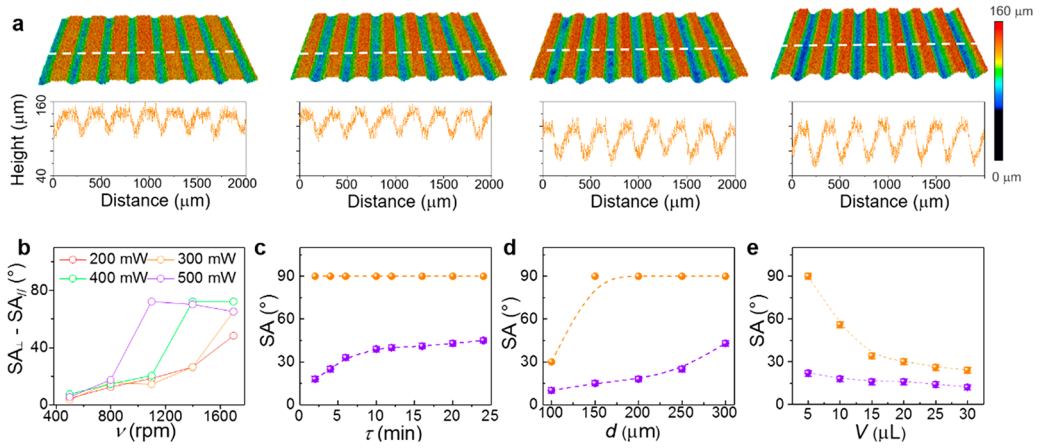

Figure 3. Optimization of anisotropic performance for smart ER-PIASS. (a) Upper row: 3D laser scanning for characterizing the profile of the resultant MG PDMS ablated by laser powers of 200, 300, 400, and 500 mW, respectively. Lower row: Line-scanning profile for presenting the topography difference of MG PDMS prepared by different laser powers. (b) ΔSA variation for water droplets (5 μL) on four different Joule-heated PIASSs using platforms ablated by (b) 200, (c) 300, (d) 400, and (e) 500 mW that are infused with paraffin wax under different thermal-spin-coating speeds ν, where the thermal-spin-coating time τ was fixed at 2 min. (c) SAs in the parallel and perpendicular directions as a function of thermal-spin-coating time, where P, ν, and V were fixed at 400 mW, 1400 rpm, and 5 μL, respectively. (d) SAs in the parallel and perpendicular directions as a function of groove's distance (d), where P, V, ν, and τ were fixed at 400 mW, 5 μL, 1400 rpm, and 2 min, respectively. (e) SAs in the parallel and perpendicular directions as a function of V, where P, d, ν, and τ were fixed at 400 mW, 150 μm, 1400 rpm, and 2 min, respectively.

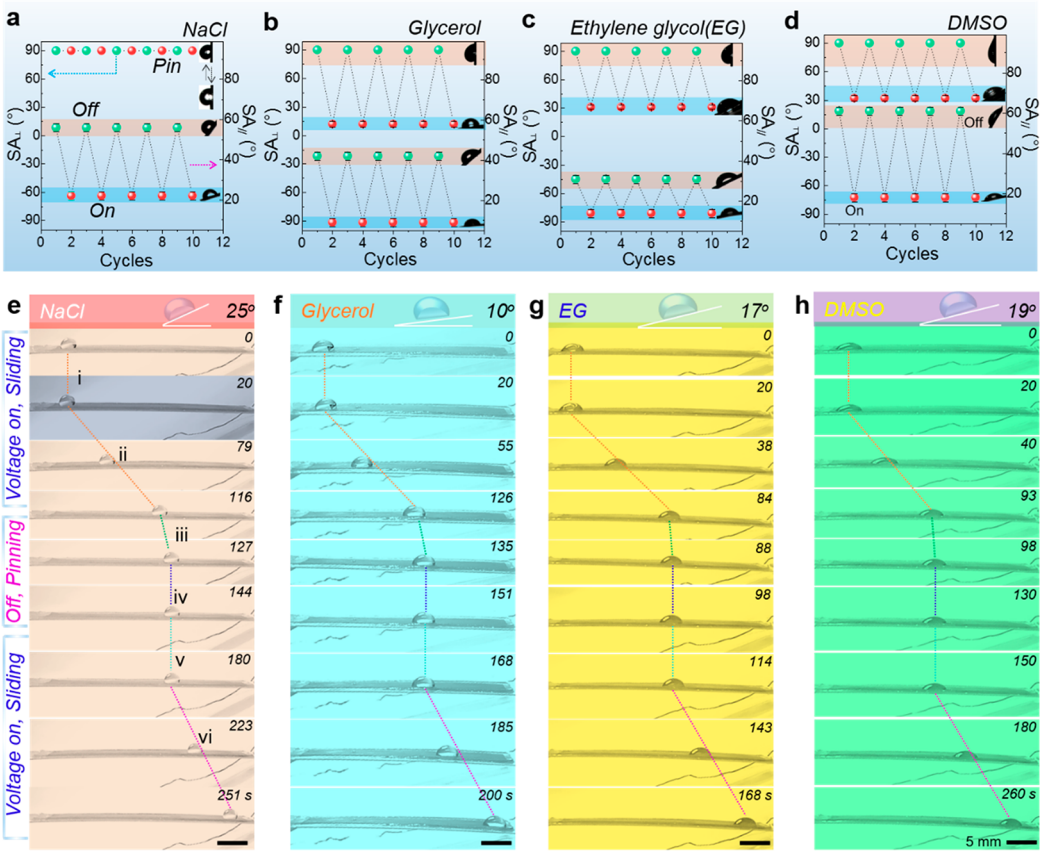

Figure 4. In situ reversible smart control for diverse liquids on ER-PIASS. (a–d) SAs in the parallel and perpendicular directions for droplets of NaCl, glycerol, ethylene glycol, and DMSO on smart PIASS in response to the cyclic pulsed electric-stimuli (5 V). Dynamic control between anisotropic sliding and pinning for droplets of (e) NaCl, (f) glycerol, (g) ethylene glycol, and (h) DMSO on smart ER-PIASS by an alternative on–off switch of an electric-trigger (5 V).

characterized h, d, and surface roughness (R_a) of the ablated anisotropic platform increased from 39.9 to 47.5, 50.3 and then 61.7 μm, from 48.1 to 52.3, 67.6 and then 68.0 μm, and from 10.6 to 12.8, 15.9 and then 18.1 μm (Figure 3a and Figure S8).

The larger the applied laser scanning power, the larger the resultant h, d, and R_a. For 5 μL droplet of water, its $SA_\perp$ and $SA_{//}$ tended to increase with the elevation of ν because of the lessened lubricant paraffin thickness leading to a larger $f_{//}$ and $f_\perp$ (Figure

DOI: 10.1021/acsami.9b17936
ACS Appl. Mater. Interfaces 2020, 12, 1895−1904

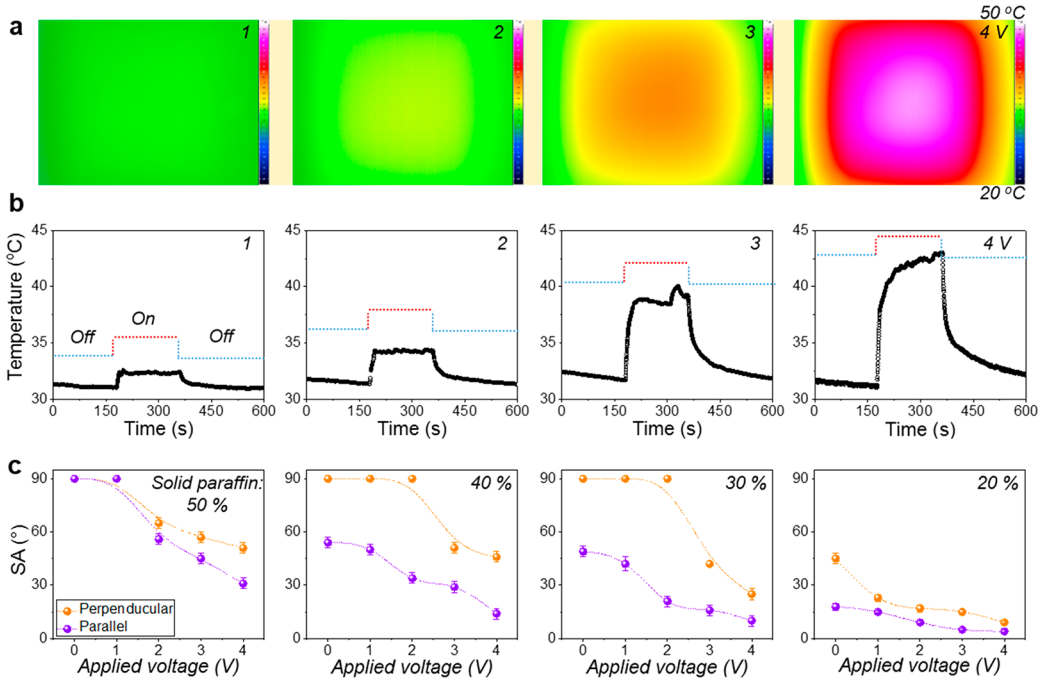

Figure 5. Tunable response-temperature of ER-PIASS toward biocompatibility. (a) Thermal images for ER-PIASS under various applied voltages of 1, 2, 3, and 4 V. (b) Temperature−time curves for ER-PIASS in response to voltages of 1, 2, 3, and 4 V. (c) SAs in the perpendicular and parallel directions as a function of voltage for four different ER-PIASSs infused by a mixture of solid/liquid paraffin, where the volume ratio for the solid/liquid paraffin was carefully blended as 1/1 (50%), 2/5 (40%), 3/10 (30%), and 1/5 (20%), respectively. The result unfolds that SAs tends to decrease with the increase of the doping content of liquid paraffin and the response temperature for a typical ER-PIASS (30%) can be tailored to 34° under an ultralow voltage of 2 V.

S9 and Figure S10a−d). The larger the applied spin-coating speed, the thinner the characterized film thickness of paraffin wax (Figures S11−14). Notably, the larger the laser scanning power, the thinner the lubricated paraffin thickness relative to the depth of grooves at a same v and thus the greater the deployed $f_{//}$ and $f_{\perp}$. Typically, when the MG PDMS platform was ablated using 400 mW, the thermal-spin-coating speed and time of the top paraffin layer were fixed at 1400 rpm and 2 min, the SAs of water droplets on Joule-heated ER-PIASS were increasing to 18° in the parallel direction and 90° (pinning) in the perpendicular direction, and so an optimized ΔSA value of 72° was harvested (Figure 3b). In addition, the τ was inversely proportional to the anisotropic degree with respect to the severe sacrifice of the top lubricant paraffin's thickness (Figure 3c and Figure S10f). The longer the applied spin-coating time, the thinner the localized film thickness of paraffin wax (Figure S15). By carefully programming the laser scanning distance, we found that the ΔSA increased from 20° to 75° at the initial stage whereas it was inclined to decrease to 72°, 65°, and then 47° with the increase of d (Figure 3d and Figure S10e). It is noteworthy that the current smart ER-PIASS tends to be more competent for manipulating droplets with smaller volumes rather than the 80 ones because the larger gravity could easily overcome the constraint force arising from the as-prepared anisotropic platform, which would be disadvantageous for the dynamic control of a drop's anisotropic sliding behavior (Figure 3e).

2.4. In Situ Reversible Droplet Motion Control on the ER-PIASS. Compared with the most previously reported smart anisotropic surfaces that are only functional for manipulating the conductive droplets,[26−28,30] the current ER-PIASS is competent for steering diverse species including conductive and non-conductive ones (Figure 4). The results showed that the droplet motion in the perpendicular direction is more difficult than that in the parallel direction on this surface. Here, in situ Joule-heat-triggered reversible switch of the droplet motion has been realized in the parallel direction on smart ER-PIASS (Supporting Information, Movies S2, S3, S4, and S5). To clarify, diverse droplet species (5 μL) on an optimized ER-PIASS (P, 400 mW; d, 150 μm; τ, 2 min; v, 1400 rpm) was selected for the following study and their reversible wettability on this smart surface had been also demonstrated (Figure S16). When the voltage was switched off, the $SA_{//}$ for water, glycerol, ethylene glycol, and DMSO was measured as 56°, 42°, 31°, and 61° (Figure 4a−d), respectively. These values would be dramatically switched to 22°, 9°, 14°, and 18° once we remotely deployed a low electric trigger (5 V) to in situ generate Joule heat for transforming the frictional ALS system to a low-adhesion ALLS one. Notably, the viscous glycerol droplet had much smaller $SA_{//}$ than three other ones because it tended to move directionally in a manner of "rolling" rather than "slipping" on such a surface.[41,42] Accordingly, smart control of the droplet motion upon switching Joule heat had been successfully implemented on the tilted ER-PIASS, where the tilt angles (TAs) for NaCl, glycerol, ethylene glycol, and DMSO were fixed at their SAs of 25°, 10°, 17°, and 19° (Figure 4e−h), respectively. Four typical stages should be introduced as follows, (i) the droplets pinned on a hot ER-PIASS when the voltage was switched on, because the surface temperature of this cold actuator would not immediately climb up to T_m until it reached the dynamic equilibrium for the heat transfer among SNWH, PDMS binder, MG PDMS, paraffin layer, and air. (ii) After tens of seconds, the continuous increase of Joule heat elevated the temperature of this cold ER-PIASS above T_m, and the melt

DOI: 10.1021/acsami.9b17936
ACS Appl. Mater. Interfaces 2020, 12, 1895−1904

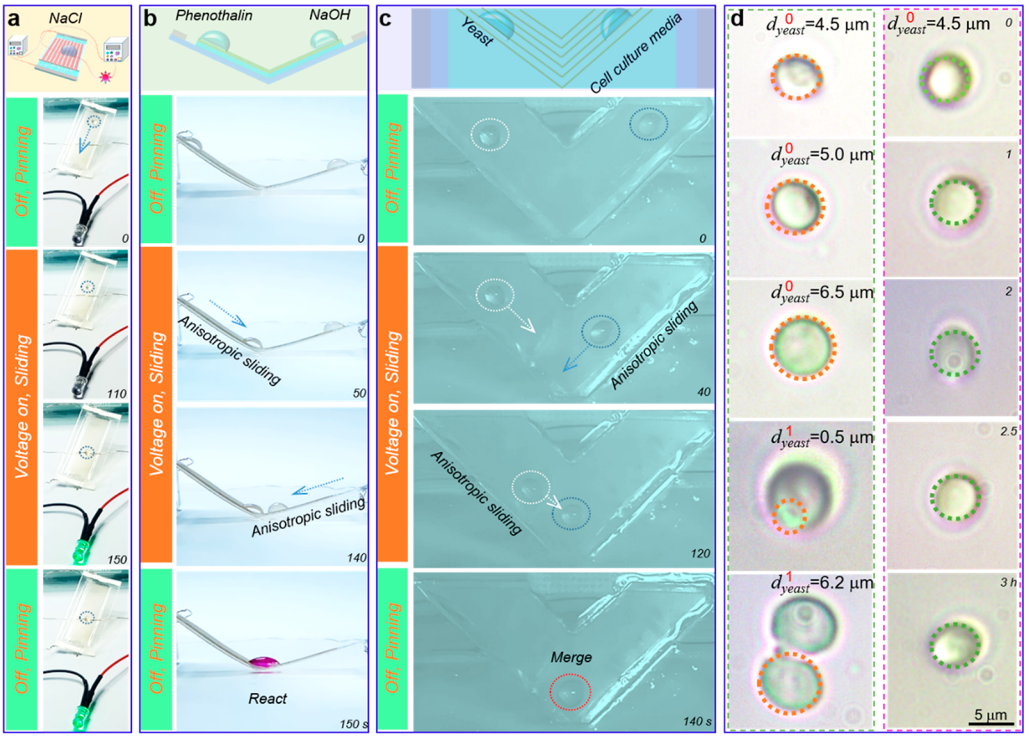

Figure 6. Smart anisotropic manipulation of diverse functionalized droplets on the low-temperature-driven ER-PIASS. (a) Intentional transport of a NaCl droplet (5 μL) on an inclined ER-PIASS (TA: 20°) toward a targeted circuit to lighten a LED lamp by one cyclic off-on−off (pinning−anisotropic sliding−pinning) operation. (b) Smart manipulation of NaOH (in DI water, 30 g L^{-1}) and phenothalin (in glycerol, 40 g L^{-1}) droplets on a curved ER-PIASS for their metachromatism. (c) Anisotropic smart control of yeast (in water, 1 g L^{-1}) and cell culture media droplets on a tilted low-temperature-driven ER-PIASS (TA: 25°) for in situ cell culture. (d) The left column indicates the evolution of the yeast cell culture in (c) and the right column represents the case of targeted therapy by directionally delivering potassium sorbate (in DI water, 20 g L^{-1}) droplet to restrain the growing yeast cells that host in cell culture media. The results unfold that this low-temperature-responsive ER-PIASS is competent for biological potential applications.

paraffin thus enabled a slippery ALLS system so as to slide a pinning droplet. (iii) Then the voltage was intentionally cut off, the melt paraffin would not solidify immediately for a frictional ALS system to brake a moving droplet until it slide for a short distance of 1 mm when the residual Joule heat in paraffin layer had been transferred to the colder sources. (iv) After a few seconds, the surface temperature decreased below T_m and one cyclic motion control of stick−slide−stick for these four liquid droplets had been successfully achieved. By the same token, another cyclic droplet motion control could be readily realized seen from cases v and vi.

2.5. SA Transitions on the ER-PIASS Induced by the Synergetic Electric-Stimulus and Liquid Paraffin Doping Ratios. For practical biological applications, people always are convinced that ER-PIASS should be capable of manipulating microfluids under a moderate temperature (e.g., 30−38 °C), which is recognized as a safety threshold that may have less side effect on the organism. In this view, we conducted experimental attempts to decrease the response temperature of ER-PIASS through modulating the lubricant recipe, that is, the volume ratio of solid and liquid paraffin. On the basis of our optimized ER-PIASS, where V, P, d, v, and τ were fixed at 5 μL, 400 mW, 150 μm, 1400 rpm, and 2 min, the effect of the doping content of liquid paraffin in the hybrid lubricant on the SAs under various electric-stimulus was deployed. Apparently, the lower response temperature should deserve a smaller applied voltage (Figure 5a). IR images unfold that the temperature plateaus of ER-PIASS under the low voltages of 1, 2, 3, and 4 V were characterized as 32.2, 34.2, 38.8, and 42.8 °C (Figure 5b), respectively. On this basis, we systematically investigated the evolution of SAs on the ER-PIASS with the increase of the doping content of liquid paraffin, which was added as 50%, 60%, 70%, and 80% (Figure 5c), respectively. Notably, the solid/liquid paraffin hybrid would not melt to modify the surface adhesions of ER-PIASS under the voltages of 1−4 V if the doping content of liquid paraffin is lower than 50% (Figure S17). SAs in the perpendicular and parallel directions were inclined to decrease with the increase of the doping content of liquid paraffin due to the gradual transition from a frictional system to a slippery one. Typically, the response temperature could be tailored to 34.2 °C under an ultralow voltage of 2 V when an optimized ΔSA of 69° was harvested through doping 70% liquid paraffin in the lubricant hybrid (Figure S18). Therein, $SA_{//}$ on this ER-PIASS could be readily switched between 49° (without electric input) and 21° (applied voltage, 2 V) while $SA_{\perp}$ was a constant of 90° (pinning). Accordingly, the ultralow-voltage-driven anisotropic smart control of liquids using this low-temperature-responsive ER-PIASS should be competent for biological applications. Notably, as the elevation of the doping content of liquid paraffin was up to 80%, the anisotropic degree of this ER-PIASS is too small to be competent for manipulating the droplet's motion.

2.6. Applications of the ER-PIASS in Manipulating Diverse Functionalized Liquids. Figure 6a presented that 5 μL droplet of NaCl pinning on smart ER-PIASS could be actuated sliding downhill directionally by virtue of remotely loading an electric-trigger of 2 V (Movie S6, Supporting Information). When it had slipped to connect two symmetric

DOI: 10.1021/acsami.9b17936
ACS Appl. Mater. Interfaces 2020, 12, 1895−1904

electrodes, the input was intentionally cut off for pinning a moving NaCl droplet so as to allow the passage of electric current and lighten a LED. The result unfolds that the dynamic control of "stick−slip-stick" using smart ER-PIASS has great potential in manipulating conductive droplets and so is adaptive for liquid-involved electric switch. In addition to a planar surface, current ER-PIASS is also demonstrated to be functional for manipulating droplets on a curved topography (Figure 6b; Movie S7, Supporting Information). In situ applying Joule heat, the pinning NaOH (in water, 5 μL) and phenothalin (in glycerol, 5 μL) droplets on the two ends of a bended ER-PIASS could be steered to coalesce and conduct the metachromatism. Notably, the response time to Joule heat for these two liquids on an identical curved PIASS displayed the apparent difference, which should be attributed to their different rheological performance. Owing to the low-temperature-driven anisotropic sliding of a drop on this smart ER-PIASS, we therefore made attempts to realize the smart dynamic control for diverse biological cells according to the aforementioned principles. Here, we successfully triggered the pinning yeast (in water, 5 μL) and cell culture media (5 μL) to slide for a merged hybrid by in situ loading an electric-stimuli of 2 V (Figure 6c; Movie S8, Supporting Information). Cell growth and cell fission could be observed from the microscope clips, which verified that the current smart ER-PIASS is applicable for biological manipulations (Figure 6d). Here, the application of in situ cell culture as a typical prototype only demonstrates that this low-temperature-driven actuator is capable of dynamically transporting the biological droplets without severe damage. The biological compatibility refers to its controlling method (e.g., low-temperature-driven controllable transportation) but not the utilized materials (e.g., paraffin wax). Utilizing this method, the yeast cell can survive in the culture medium on this low-temperature-driven smart surface, indicating that this controlling method has biological compatibility without damaging the manipulated biological ones. By the same token, we could manipulate the potassium sorbate droplet (in DI water, 5 μL) to blend with an as-prepared mixture of yeast and cell culture media for restraining the cell growth and fission processes (Figure S19; Movie S9, Supporting Information).

3. CONCLUSIONS

In summary, a new kind of hydrophobic anisotropic MG PDMS platform has been manufactured by one-step programmable femtosecond laser scanning. Upon a facile thermal-spin-coating method, the solid paraffin can be uniformly coated on the as-prepared MG PDMS for temperature-responsive PIASS. By incorporation of an embedded flexible SNWH, smart ER-PIASS with excellent durability is therefore harvested. By remotely loading/discharging an electric-trigger, the dynamic control between anisotropic sliding and pinning for diverse liquids has been realized. The principle is that the electric-induced Joule heat transfers to melt the surface paraffin of ER-PIASS within 20 s for a slippery ALLS system when we simply apply an electric-stimuli of 5 V. Once the voltage is intentionally discharged, the melt paraffin would rapidly solidify to an ALS system within 10 s for pinning a sliding droplet on ER-PIASS. Additionally, we quantitatively investigate the contributions of P, d, V, v, and τ to the ΔSA values of droplets on ER-PIASSs. The optimized ΔSA of 75° can be therefore obtained, which is highly superior/comparable to the anisotropic degree of the previously reported studies. Owing to its outstanding flexibility, in situ anisotropic manipulation of droplets on a curved ER-PIASS for metachromatism has been successfully deployed. Significantly, current low-temperature-driven ER-PIASS having merits of biocompatibility enables us to realize the anisotropic smart control of cell culture medium and yeast droplets for their directional coalesce, growth and fission. Compared with previous electric/photoresponsive anisotropic surfaces, current ER-PIASS is more competent for in situ manipulating diverse liquids including conductive and nonconductive ones and suitable for a variety of materials, which is very crucial for broad applications. This work gives insights for designing temperature-responsive smart surfaces for smart control of diverse drop's anisotropic sliding and microfluidics and biological applications on 2D/3D surfaces.

4. EXPERIMENTAL SECTION

4.1. Materials. The PDMS (Sylgard 184 Kit, Dow Corning) membranes were prepared by spin-coating (time, 30 s; speed, 500 rpm) the mixture of prepolymer and cross-linker (v/v, 10:1) on a glass platform. After degasification for about 30 min, the mixture was then cured in a heating oven for 0.5 h at 100 °C. Finally, it was cut into pieces (5 × 3 cm^2) for laser processing. $AgNO_3$ (99.8%) was obtained from Shanghai Qiangshun Chemical Reagent Co., Ltd. Paraffin wax (chunks, T_m ~ 40−42°), polyvinylpyrrolidone (PVP, MW of 55 000) and hydroxypropyl methylcellulose (HPMC) were purchased from Sigma-Aldrich. Ethylene glycol, glycerol, dimethyl sulfoxide (DMSO), potassium sorbate, sodium hydroxide, NaCl, NaBr, and acetone were donated from Sinopharm Chemical Reagent Co., Ltd. Sago 9760 and Sago 3223 were obtained from Sago Co., Ltd. Distilled water (H_2O, 1 g cm^{-3} density) served as contact-angle test materials.

4.2. Femtosecond Laser Fabrication. The microgrooved (MG) polydimethylsiloxane (PDMS) films were manufactured by the line-by-line scanning of femtosecond laser. The laser beam (104 fs, 1 kHz, 800 nm) from a regenerative amplified Ti:sapphire femtosecond laser system (Legend Elite-1K-HE, Coherent) was employed for ablation. During the fabrication process, the laser beam was guided onto the PDMS surface via a galvanometric scanning system (SCANLAB), which made the laser beam focus and scan along the x/y coordinate direction. The scanning spacing between two adjacent lines ranged from 100 to 300 μm. The laser power ranged from 200 to 500 mW, and the scanning speed was 2 mm/s.

4.3. Fabrication of Smart ER-PIASS. *Synthesis of High-Quality SNWs.* For synthesis, (A) 0.220 M NaBr, (B) 0.210 M NaCl, and (C) 0.505 M PVP in EG were individually prepared for utilization. Fresh AgNO3 was dissolved in EG in an ice-cold ultrasonic bath (4−8 °C) for 5 min. Subsequently 2.5 mL of A, 5 mL of B, 25 mL of C, and 25 mL of $AgNO_3$ (0.265 M) were successively added to a 100 mL flask placed in an oil bath at room temperature. Vigorous stirring was applied for 30 min, and then the temperature in the flask was elevated to 170 °C in 15 min, where the nitrogen gas with a flux of 150 mL min^{-1} was bubbled through the reaction. Thereafter, the flask was corked, and the reaction was left for 1 h without disturbing. The flask was taken off from the oil bath immediately and transferred to the water for cooling once the reaction was terminated.[38]

Formulation of SNW Ink. A total of 16 mg of purified SNWs harvested by a positive-pressure filtration and acetone purification procedure was dissolved in 16 mL of DI water with the assistance of 32 mg of HPMC and a Sago-dispersant (v/v 0.0025%) and a Sago-flatting agent (v/v 0.0025%). Finally, 1 mg mL^{-1} SNW ink could be obtained after the mixture was fixed on a table concentrator and allowed to blend for 1.5 h with a rotating speed of 110 rpm.[37,39]

Preparation of Flexible SNWH. An automatic coating machine (BEVS 1811/2) equipped with an OSP-30 scraper was utilized to coat the conductive SNW network on flexible PET substrate, where the coating rate and area were fixed at 100 mm s^{-1} and A4 (21.0 cm × 29.7 cm), respectively. The starting button was pressed after the dropping of 1 mL of SNW ink and highly conductive SNW films were obtained after a brief annealing process at 60 °C for 5 min. Thereafter, two symmetric copper-wire electrodes could be soldered using patterned oblong silver

DOI: 10.1021/acsami.9b17936
ACS Appl. Mater. Interfaces 2020, 12, 1895−1904

paste. SNWH could be prepared after annealing at 70 °C for 5 h, which was then integrated to MG PDMS through a thin layer of PDMS binder (thickness, ∼50 μm). In regard of the method for SNWH embedded in the MG-PDMS, we first coated a thin layer (dry film thickness, ∼50 μm) of wet PDMS sol−gel on the SNWH by spin-coating (speed, 300 rpm; time, 30 s). Thereafter, the MG PDMS was put on SNWH with a thin layer of wet PDMS binder, which was then suffered from vacuum-pumping and heating (80 °C, 1 h) processes for the success fabrication of ER-PIASS.

Thermal-Spin-Coating of Paraffin Wax. The MG PDMS with an embedded SNWH was fixed on a glass slide by 3 M adhesive tape. Then, a patch of solid paraffin wax was put on this surface and allowed to melt and spread for 2 min under the assistance of a top infrared radiation (IR) lamp, where the distance between the IR lamp and sample were fixed at ∼10 cm. Thereafter, a spin-coating program (time, 2−24 min; speed, 500−1700 rpm) was initiated. Finally, Smart ER-PIASS composed of top paraffin layer, MG PDMS, PDMS binder, and underlying SNWH could be obtained after a condensation process at room temperature.

4.4. Characterization. The micro- and nanostructures induced by the laser were characterized by using a field-emission scanning electron microscope (JSM-6700F). The contact angles of the water droplet, NaCl, glycerol, DMSO, and EG in air were measured using a CA100C contact-angle system (Innuo) with the sessile drop method. The average values were obtained by measuring five drops at different locations on the same surface. All of the contact-angle measurements were conducted at 10% humidity and 20 °C. The sheet resistance of SNW film were measured using a four-point probe technique (RST-9, Four-Probe Technology). The surface temperatures of the SNWH and DMCA were measured by a thermal infrared camera (VarioCAMhr head 680, InfraTec).

■ ASSOCIATED CONTENT

Supporting Information

See Supporting Information for the The Supporting Information is available free of charge at https://pubs.acs.org/doi/10.1021/acsami.9b17936.

High-resolution SEM images for laser-ablated micro- and nanostructures on MG PDMS, digital picture for a home-built thermal-spin-coating facility composed of a top IR lamp and a spin-coater equipped with a vac-sorb pump, statistic sheet resistance of the resultant silver nanowire conductive film, morphology investigation for MG PDMS fabricated by various laser power, in situ reversible wettability for diverse liquids on ER-PIASS, the proof-of-concept "targeted therapy" by current low-temperature-driven ER-PIASS, variations of SAs on the ER-PIASS (the doping content of liquid paraffin in the hybrid lubricant: 40%) with the applied voltage, in addition to the evolution of ΔSAs on the ER-PIASSs with the increase of the doping content of liquid paraffin in the hybrid lubricant (PDF)

Transparent, conductive, and flexible SNWH (MP4)

NaCl droplet with electric-trigger on, pinning to slidding; electric-trigger off, sliding to pinning; electric-trigger on, pinning to slidding (MP4)

Glycerol droplet with electric-trigger on, pinning to slidding; electric-trigger off, sliding to pinning; electric-trigger on, pinning to slidding (MP4)

Ethylene glycol droplet electric-trigger on, pinning to slidding; electric-trigger off, sliding to pinning; electric-trigger on, pinning to slidding (MP4)

DMSO droplet electric-trigger on, pinning to slidding; electric-trigger off, sliding to pinning; electric-trigger on, pinning to slidding (MP4)

Voltage on, NaCl droplet was activated from pinning to anistropic sliding; voltage off, NaCl droplet pinned between two Cu wires to lighten an LED lamp (MP4)

Voltage on, two droplets were triggered from pinning to anistropic sliding for coalesce on a curved PIASS (MP4)

Voltage on, two droplets were actuated from pinning to anistropic sliding for biological cell culture(MP4)

Voltage on, two droplets were actuated from pinning to anistropic sliding for restainng the biological cell growth (MP4)

■ AUTHOR INFORMATION

Corresponding Authors

*E-mail: huyl@ustc.edu.cn.

*E-mail: dongwu@ustc.edu.cn.

ORCID

Jiawen Li: 0000-0003-3950-6212

Yanlei Hu: 0000-0003-1964-0043

Dong Wu: 0000-0003-0623-1515

Jiaru Chu: 0000-0001-6472-8103

Notes

The authors declare no competing financial interest.

■ ACKNOWLEDGMENTS

Fundamental Research Funds for the Central Universities (Nos. WK2090090024, WK6030000113, WK2090090025), Chinese Academy of Sciences Instrument Project (YZ201566), the National Natural Science Foundation of China (Nos. 51805508, 61505047, 51605463, 61675190, and 51675503), and the China Postdoctoral Science Foundation (No. BH2090000025, 2018M642534).

■ REFERENCES

(1) Vogel, N.; Belisle, R. A.; Hatton, B.; Wong, T. S.; Aizenberg, J. Transparency and Damage Tolerance of Patternable Omniphobic Lubricated Surfaces Based on Inverse Colloidal Monolayers. *Nat. Commun.* **2013**, *4*, 2176.

(2) Wong, T. S.; Kang, S. H.; Tang, S. K.; Smythe, E. J.; Hatton, B. D.; Grinthal, A.; Aizenberg, J. Bioinspired Self-Repairing Slippery Surfaces with Pressure-Stable Omniphobicity. *Nature* **2011**, *477*, 443−447.

(3) Yao, X.; Song, Y.; Jiang, L. Applications of Bio-Inspired Special Wettable Surfaces. *Adv. Mater.* **2011**, *23*, 719−734.

(4) Yao, X.; Hu, Y.; Grinthal, A.; Wong, T. S.; Mahadevan, L.; Aizenberg, J. Adaptive Fluid-Infused Porous Films with Tunable Transparency and Wettability. *Nat. Mater.* **2013**, *12*, 529−534.

(5) Yu, C.; Zhu, X.; Li, K.; Cao, M.; Jiang, L. Manipulating Bubbles in Aqueous Environment *via* a Lubricant-Infused Slippery Surface. *Adv. Funct. Mater.* **2017**, *27*, 1701605.

(6) Hou, X.; Hu, Y.; Grinthal, A.; Khan, M.; Aizenberg, J. Liquid-Based Gating Mechanism with Tunable Multiphase Selectivity and Antifouling Behaviour. *Nature* **2015**, *519*, 70−73.

(7) Hou, X. Smart Gating Multi-Scale Pore/Channel-Based Membranes. *Adv. Mater.* **2016**, *28*, 7049−7064.

(8) Anand, S.; Paxson, A. T.; Dhiman, R.; Smith, J. D.; Varanasi, K. K. Enhanced Condensation on Lubricant-Impregnated Nanotextured Surfaces. *ACS Nano* **2012**, *6*, 10122−10129.

(9) Park, K. C.; Kim, P.; Grinthal, A.; He, N.; Fox, D.; Weaver, J. C.; Aizenberg, J. Condensation on Slippery Asymmetric Bumps. *Nature* **2016**, *531*, 78.

(10) Wang, Y.; Zhang, H.; Liu, X.; Zhou, Z. Slippery Liquid-Infused Substrates: A Versatile Preparation, Unique Anti-Wetting and Drag-Reduction Effect on Water. *J. Mater. Chem. A* **2016**, *4*, 2524−2529.

(11) Manna, U.; Raman, N.; Welsh, M. A.; Zayas-Gonzalez, Y. M.; Blackwell, H. E.; Palecek, S. P.; Lynn, D. M. Slippery Liquid-Infused

DOI: 10.1021/acsami.9b17936
ACS Appl. Mater. Interfaces 2020, 12, 1895−1904

Porous Surfaces that Prevent Microbial Surface Fouling and Kill Non-Adherent Pathogens in Surrounding Media: A Controlled Release Approach. *Adv. Funct. Mater.* **2016**, *26*, 3599−3611.
(12) Yin, J.; Mei, M.; Li, Q.; Xia, R.; Zhang, Z.; Chu, C. Self-Cleaning and Antibiofouling Enamel Surface by Slippery Liquid-Infused Technique. *Sci. Rep.* **2016**, *6*, 25924.
(13) Sunny, S.; Cheng, G.; Daniel, D.; Lo, P.; Ochoa, S.; Howell, C.; Vogel, N.; Majid, A.; Aizenberg, J. Transparent Antifouling Material for Improved Operative Field Visibility in Endoscopy. *Proc. Natl. Acad. Sci. U. S. A.* **2016**, *113*, 11676−11681.
(14) Kim, P.; Wong, T. S.; Alvarenga, J.; Kreder, M. J.; AdornoMartinez, W. E.; Aizenberg, J. Liquid-Infused Nanostructured Surfaces with Extreme Anti-Ice and Anti-Frost Performance. *ACS Nano* **2012**, *6*, 6569−6577.
(15) Lv, J.; Song, Y.; Jiang, L.; Wang, J. Bio-Inspired Strategies for Anti-Icing. *ACS Nano* **2014**, *8*, 3152−3169.
(16) Subramanyam, S. B.; Rykaczewski, K.; Varanasi, K. K. Ice Adhesion on Lubricant-Impregnated Textured Surfaces. *Langmuir* **2013**, *29*, 13414−13418.
(17) Lee, J.; Shin, S.; Jiang, Y.; Jeong, C.; Stone, H. A.; Choi, C. H. Oil-Impregnated Nanoporous Oxide Layer for Corrosion Protection with Self-Healing. *Adv. Funct. Mater.* **2017**, *27*, 1606040.
(18) Leslie, D. C.; Waterhouse, A.; Berthet, J. B.; Valentin, T. M.; Watters, A. L.; Jain, A.; Kim, P.; Hatton, B. D.; Nedder, A.; Donovan, K.; Super, E. H.; Howell, C.; Johnson, C. P.; Vu, T. L.; Bolgen, D. E.; Rifai, S.; Hansen, A. R.; Aizenberg, M.; Super, M.; Aizenberg, J.; Ingber, D. E. A Bioinspired Omniphobic Surface Coating on Medical Devices Prevents Thrombosis and Biofouling. *Nat. Biotechnol.* **2014**, *32*, 1134.
(19) Bohn, H. F.; Federle, W. Insect Aquaplaning: Nepenthes Pitcher Plants Capture Prey with the Peristome, A Fully Wettable Water-Lubricated Anisotropic Surface. *Proc. Natl. Acad. Sci. U. S. A.* **2004**, *101*, 14138−14143.
(20) Chen, H.; Zhang, P.; Zhang, L.; Liu, H.; Jiang, Y.; Zhang, D.; Han, Z.; Jiang, L. Continuous Directional Water Transport on the Peristome Surface of Nepenthes Alata. *Nature* **2016**, *532*, 85−89.
(21) Zhang, P.; Liu, H.; Meng, J.; Yang, G.; Liu, X.; Wang, S.; Jiang, L. Grooved Organogel Surfaces towards Anisotropic Sliding of Water Droplets. *Adv. Mater.* **2014**, *26*, 3131−3135.
(22) Yong, J.; Yang, Q.; Chen, F.; Zhang, D.; Farooq, U.; Du, G.; Hou, X. A Simple Way to Achieve Superhydrophobicity, Controllable Water Adhesion, Anisotropic Sliding, and Anisotropic Wetting Based on Femtosecond-Laser-Induced Line-Patterned Surfaces. *J. Mater. Chem. A* **2014**, *2*, 5499−5507.
(23) Huang, S.; Li, J.; Liu, L.; Zhou, L.; Tian, X. Lossless Fast Drop Self-Transport on Anisotropic Omniphobic Surfaces: Origin and Elimination of Microscopic Liquid Residue. *Adv. Mater.* **2019**, *31*, 1901417.
(24) Chen, X.; Ren, K.; Wang, J.; Lei, W.; Ji, J. Infusing Lubricant onto Erasable Microstructured Surfaces toward Guided Sliding of Liquid Droplets. *ACS Appl. Mater. Interfaces* **2017**, *9*, 1959−1967.
(25) Kamei, J.; Yabu, H. On-Demand Liquid Transportation Using Bioinspired Omniphobic Lubricated Surfaces Based on Self-Organized Honeycomb and Pincushion Films. *Adv. Funct. Mater.* **2015**, *25*, 4195−4201.
(26) Guo, T.; Che, P.; Heng, L.; Fan, L.; Jiang, L. Anisotropic Slippery Surfaces: Electric-Driven Smart Control of a Drop's Slide. *Adv. Mater.* **2016**, *28*, 6999−7007.
(27) Che, P.; Heng, L.; Jiang, L. Lubricant-Infused Anisotropic Porous Surface Design of Reduced Graphene Oxide Toward Electrically Driven Smart Control of Conductive Droplets' Motion. *Adv. Funct. Mater.* **2017**, *27*, 1606199.
(28) Wang, Z.; Heng, L.; Jiang, L. Effect of Lubricant Viscosity on the Self-Healing Properties and Electrically Driven Sliding of Droplets on Anisotropic Slippery Surfaces. *J. Mater. Chem. A* **2018**, *6*, 3414−3421.
(29) Wang, L.; Heng, L.; Jiang, L. Temperature-Responsive Anisotropic Slippery Surface for Smart Control of the Droplet Motion. *ACS Appl. Mater. Interfaces* **2018**, *10*, 7442−7450.
(30) Wang, Z.; Liu, Y.; Guo, P.; Heng, L.; Jiang, L. Photoelectric Synergetic Responsive Slippery Surfaces Based on Tailored Anisotropic Films Generated by Interfacial Directional Freezing. *Adv. Funct. Mater.* **2018**, *28*, 1801310.
(31) Yin, K.; Yang, S.; Dong, X.; Chu, D.; Duan, J.-A.; He, J. Robust Laser-Structured Asymmetrical PTFE Mesh for Underwater Directional Transportation and Continuous Collection of Gas Bubbles. *Appl. Phys. Lett.* **2018**, *112*, 243701.
(32) Duan, J.-A.; Dong, X.; Yin, K.; Yang, S.; Chu, D. A Hierarchical Superaerophilic Cone: Robust Spontaneous and Directional Transport of Gas Bubbles. *Appl. Phys. Lett.* **2018**, *113*, 203704.
(33) Yin, K.; Du, H.; Dong, X.; Wang, C.; Duan, J.-A.; He, J. A Simple Way to Achieve Bioinspired Hybrid Wettability Surface with Micro/Nanopatterns for Efficient Fog Collection. *Nanoscale* **2017**, *9*, 14620−14626.
(34) Yin, K.; Chu, D.; Dong, X.; Wang, C.; Duan, J.-A.; He, J. Femtosecond Laser Induced Robust Periodic Nanoripple Structured Mesh for Highly Efficient Oil-Water Separation. *Nanoscale* **2017**, *9*, 14229−14235.
(35) Meng, X.; Wang, Z.; Wang, L.; Heng, L.; Jiang, L. A Stable Solid Slippery Surface with Thermally Assisted Self-Healing Ability. *J. Mater. Chem. A* **2018**, *6*, 16355−16360.
(36) Manabe, K.; Matsubayashi, T.; Tenjimbayashi, M.; Moriya, T.; Tsuge, Y.; Kyung, K.-H.; Shiratori, S. Controllable Broadband Optical Transparency and Wettability Switching of Temperature-Activated Solid/Liquid-Infused Nanofibrous Membranes. *ACS Nano* **2016**, *10*, 9387−9396.
(37) Chen, C.; Zhao, Y.; Wei, W.; Tao, J.; Lei, G.; Jia, D.; Wan, M.; Li, S.; Ji, S.; Ye, C. Fabrication of Silver Nanowire Transparent Conductive Films with an Ultra-Low Haze and Ultra-High Uniformity and Their Application in Transparent Electronics. *J. Mater. Chem. C* **2017**, *5*, 2240−2246.
(38) Jia, D.; Zhao, Y.; Wei, W.; Chen, C.; Lei, G.; Wan, M.; Tao, J.; Li, S.; Ji, S.; Ye, C. Synthesis of Very Thin Ag Nanowires with Fewer Particles by Suppressing Secondary Seeding. *CrystEngComm* **2017**, *19*, 148−153.
(39) Chen, C.; Huang, Z.; Jiao, Y.; Shi, L.-A.; Zhang, Y.; Li, J.; Li, C.; Lv, X.; Wu, S.; Hu, Y.; Zhu, W.; Wu, D.; Chu, J.; Jiang, L. In Situ Reversible Control between Sliding and Pinning for Diverse Liquids under Ultra-Low Voltage. *ACS Nano* **2019**, *13*, 5742−5752.
(40) Ji, S.; He, W.; Wang, K.; Ran, Y.; Ye, C. Thermal Response of Transparent Silver Nanowire/PEDOT:PSS Film Heaters. *Small* **2014**, *10*, 4951−4960.
(41) Smith, J. D.; Dhiman, R.; Anand, S.; Reza-Garduno, E.; Cohen, R. E.; McKinley, G. H.; Varanasi, K. K. Droplet Mobility on Lubricant-Impregnated Surfaces. *Soft Matter* **2013**, *9*, 1772−1780.
(42) Yokoyama, K.; Sakai, M.; Isobe, T.; Matsushita, S.; Nakajima, A. Droplet Viscosity Effects on Dynamic Hydrophobicity of a Solid-Liquid Bulk Composite Prepared from Porous Glass. *J. Mater. Sci.* **2017**, *52*, 595−604.

DOI: 10.1021/acsami.9b17936
ACS Appl. Mater. Interfaces 2020, 12, 1895−1904